One-Bit Phase Retrieval: More Samples Means Less Complexity?

Arian Eamaz, *Student Member, IEEE*, Farhang Yeganegi, and Mojtaba Soltanalian, *Senior Member, IEEE*

Abstract—The classical problem of phase retrieval has found a wide array of applications in optics, imaging and signal processing. In this paper, we consider the phase retrieval problem in a one-bit setting, where the signals are sampled using onebit analog-to-digital converters (ADCs). A significant advantage of deploying one-bit ADCs in signal processing systems is their superior sampling rates as compared to their high-resolution counterparts. This leads to an enormous amount of one-bit samples gathered at the output of the ADC in a short period of time. We demonstrate that this advantage pays extraordinary dividends when it comes to convex phase retrieval formulationsnamely that the often encountered matrix semi-definiteness constraints as well as rank constraints (that are computationally prohibitive to enforce), become redundant for phase retrieval in the face of a growing sample size. Several numerical results are presented to illustrate the effectiveness of the proposed methodologies.

Index Terms—Convex optimization, one-bit ADCs, phase retrieval, semi-definite relaxation, statistical signal processing.

I. INTRODUCTION

PHASE retrieval has gained significant interest in applied physics and statistical signal processing communities over the past decades [1]–[21]. This classical problem manifests as the recovery of an unknown signal solely from phaseless measurements that depend on the signal through a linear observation model. Due to the intrinsic difficulties of the recovery task [22], recently, there have been many efforts to propose approximate or relaxed versions of the phase retrieval problem in a convex optimization language, particularly via semi-definite programming [11], [23].

Quantization of the signals of interest through analog-to-digital converters (ADCs) is an important task in digital signal processing applications. A very large number of quantization levels is necessary in order to represent the original continuous signal in high-resolution scenarios. The large number of quantization bits, however, can cause a considerable increase in the overall power consumption and the manufacturing cost of ADCs, as well as a reduction in sampling rate [24]. Such disadvantages have motivated the researchers to investigate the idea of utilizing fewer bits for sampling. *One-bit quantization* is an extreme quantization scenario, in which the signals are compared with given threshold levels at the ADCs, producing sign (±1) outputs. This enables signal processing equipments

This work was supported in part by the National Science Foundation Grant CCF-1704401.

A. Eamaz, F. Yeganegi and M. Soltanalian are with the Department of Electrical and Computer Engineering, University of Illinois Chicago, Chicago, IL 60607, USA (*Corresponding author: Arian Eamaz*).

to sample at a very high rate, with a considerably lower cost and energy consumption, compared to their counterparts which employ multi-bit ADCs [24]–[27]. We further note that one-bit quantization with a fixed threshold (usually zero) can lead to difficulties in the estimation of the signal amplitude. Employing time-varying thresholds, however, has been shown to result in enhanced signal recovery performance in some recent works [24], [28]–[33].

A. Contributions of the Paper

While convex formulations of the phase retrieval problem promise a global solution, some of the introduced constraints are computationally costly; including the matrix rank and the positive semi-definite (PSD) constraints. However, we show that if more samples are available, the sheer number of samples can constrain the solution in a less costly manner and make such constraints redundant. Note that, as mentioned earlier, by employing the one-bit quantization, sampling can be done at significantly higher rates. As a result, the emergence of one-bit sampling techniques paves the way for an investigation on the role of an increased sample size in the phase retrieval problem.

In this paper, we show that the phase retrieval problem can be tackled by taking advantage of the large number of linear observation inequalities that emerge naturally in the one-bit quantization regimen. Instead of considering the often-formulated trace relaxation problem, our approach to one-bit phase retrieval is presented as a randomized Kaczmarz algorithm-based recovery. We present our results on a proper selection of the sufficient number of samples. Furthermore, an algorithm is proposed based on our model to adaptively evaluate the time-varying sampling thresholds. The performance of our approach with an increased sample size is also investigated when noisy measurements are utilized.

B. Organization of the Paper

Since our approach takes root in convex phase retrieval, Section II is dedicated to a survey of such formulations. In Section III, we will discuss the appearance of one-bit sampling with time-varying thresholds in the phase retrieval context through linear inequality constraints (defining a polyhedron feasible region), as well as the randomized Kaczmarz algorithm (RKA) that can be utilized to recover our desired signal. To investigate the error recovery of the proposed algorithm, a theorem, which may be useful to select the number of measurement, is presented in Section IV. Section V is devoted to comparing our method with PhaseLift, its one-bit version

and Wirtinger flow (WirtFlow) in terms of their computational burden. Based on our proposed polyhedron formulation, an algorithm is proposed to obtain the adaptive time-varying thresholds which benefit finding the signal of interest with more accuracy and less computational cost in Section VI. In Section VII, the noisy measurement scenario is studied owing to its importance in practical applications. Finally, Section IX concludes the paper.

Notation: We use bold lowercase letters for vectors and bold uppercase letters for matrices. \mathbb{C} and \mathbb{R} represent the set of complex and real numbers, respectively. $(\cdot)^{\top}$ and $(\cdot)^{\mathrm{H}}$ denote the vector/matrix transpose, and the Hermitian transpose, respectively. $I_N \in \mathbb{R}^{N \times N}$ is the identity matrix of size N. Tr(.) denotes the trace of the matrix argument. The spectral radius $\rho(B)$ of a matrix B is defined as a maximum absolute value of its eigenvalues [34]. The Frobenius norm of a matrix $m{B} \in \mathbb{C}^{M \times N}$ is defined as $\| m{B} \|_{\mathrm{F}} = \sqrt{\sum_{r=1}^{M} \sum_{s=1}^{N} \left| b_{rs} \right|^2}$ where $\{b_{rs}\}$ are elements of $m{B}$. The ℓ^k -norm for a vector **b** is defined as $\|\mathbf{b}\|_{k}^{k} = \sum_{i} b_{i}^{k}$. The Hadamard (element-wise) product of two matrices B_1 and B_2 is denoted as $B_1 \odot B_2$. Additionally, the Kronecker product is denoted as $B_1 \otimes B_2$. The vectorized form of a matrix B is written as vec(B). $\mathbf{1}_s$ is a s-dimensional all-one vector. Given a scalar x, we define $(x)^+$ as $\max\{x,0\}$. For an event \mathcal{E} , $\mathbb{I}_{(\mathcal{E})}$ is the indicator function for that event meaning that $\mathbb{I}_{(\mathcal{E})}$ is 1 if \mathcal{E} occurs, and 0 otherwise. $f \approx g$ means f and g are asymptotically equal. The cumulative distribution function (CDF) of the zero-mean Gaussian process $z \sim \mathcal{N}(0,\zeta)$ is given by

$$\Phi(z) \triangleq \frac{1}{\sqrt{2\pi}} \int_{-\infty}^{z} e^{-\frac{t^2}{2\zeta^2}} dt.$$
 (1)

To compare two different CDFs, the Hellinger distance may be utilized [35], which is defined as

$$d_H^2\left(p,q\right) \triangleq \left(\sqrt{p} - \sqrt{q}\right)^2 + \left(\sqrt{1-p} - \sqrt{1-q}\right)^2, \quad (2)$$
 with $p, q \in [0, 1]$.

II. CONVEX PHASE RETRIEVAL: OPPORTUNITIES AND CHALLENGES

To tackle the phase retrieval problem, many non-convex and local optimization algorithms have been developed over the years. Recently, however, convex programming formulations have come to the fore to yield *global* solutions. As a case in point, the *PhaseLift* method in [11] adopts a convex optimization mathematical machinery to tackle the phase retrieval problem, ensuring a near exact recovery of the unknown signal. To do so, PhaseLift relies on a trace-norm relaxation that is used in lieu of the original non-convex rank minimization problem—more on this below. Due to the imposition of the positive semi-definite (PSD) constraint, the PhaseLift problem formulation joins the class of semi-definite programs (SDPs).

Suppose $\mathbf{x} \in \mathbb{C}^n$ is the discrete signal of interest that is observed linearly through the lens of sensing vectors a_j , with $\left\{a_j^{\mathrm{H}}\right\}$ constituting the rows of the sensing matrix $\mathbf{A} \in \mathbb{C}^{m \times n}$. Our goal in phase retrieval is to recover the signal \mathbf{x} from phaseless measurements y_i [11], [23]:

$$y_j = |\mathbf{a}_j^{\mathrm{H}} \mathbf{x}|, \quad j \in \mathcal{J} = \{1, \dots, m\}.$$
 (3)

To ease the mathematical manipulation, one can use the squared version of (3), i.e.,

$$y_j^2 = \mathbf{x}^{\mathrm{H}} \mathbf{a}_j \mathbf{a}_j^{\mathrm{H}} \mathbf{x},$$

= $\mathrm{Tr} \left(\mathbf{a}_j \mathbf{a}_j^{\mathrm{H}} \mathbf{x} \mathbf{x}^{\mathrm{H}} \right),$
= $\mathrm{Tr} \left(\mathbf{V}_j \mathbf{X} \right),$ (4)

where $X = \mathbf{x}\mathbf{x}^{\mathrm{H}}$ and $V_j = a_j a_j^{\mathrm{H}}$. Based on (4), the phase retrieval problem can be defined as,

find
$$X$$

s.t. $\operatorname{Tr}(V_{j}X) = y_{j}^{2}$,
 $\operatorname{rank}(X) = 1$,
 $X \succ 0$. (5)

To have a convex program as [11], the problem (5) is then relaxed as [11],

$$\begin{aligned} & \min_{\boldsymbol{X}} & \operatorname{Tr}(\boldsymbol{X}) \\ & \text{s.t.} & \operatorname{Tr}(\boldsymbol{V}_{j}\boldsymbol{X}) = y_{j}^{2}, \\ & \boldsymbol{X} \succeq 0. \end{aligned} \tag{6}$$

The linear objective and constraints, along with the PSD constraint, turns (6) to a semi-definite program which is convex [36]. Due to its convexity, there exists a wide array of numerical solvers including the popular Nesterov's accelerated first-order method to tackle the problem above [23], [37].

Although, the rank-one and the PSD constraints are deemed necessary to the phase retrieval formulation, they lead to an increased computational cost even in cases where we deal with a convex optimization landscape. To enforce the PSD constraint, a projected gradient method is used in [23], where the approximate solution should be projected onto a PSD cone at each iteration by recovering all eigenvalues and setting the negative eigenvalues to zero, which is quite expensive [23].

An interesting alternative to enforcing the PSD constraint in (6) emerges when one increases the number of samples m, and solves the overdetermined linear system of equations with $m \geq n$. By collecting a large number of samples, the linear constraints $\operatorname{Tr}(V_jX) = y_j^2$ may actually yield the optimum inside the PSD area $X \succeq 0$. As a result of increasing the number of samples, it is possible that the intersection of these hyperplanes will shrink to the optimal point without the need to consider the PSD constraint. However, this idea may face practical limitations in the case of multi-bit quantization systems since ADCs capable of ultra-high rate sampling are difficult and expensive to produce. Moreover, one cannot necessarily expect these constraints to intersect with the PSD cone in such a way to form a finite-volume space before the optimum is obtained [11].

As we will show in the next section, by defining the phase retrieval in the one-bit sampling regimen, linear equality constraints are superseded with linear inequalities. Therefore, by increasing the number of samples, we may create a finite-volume space inside the cone $X \succeq 0$; making the PSD constraint no longer informative or required. From a practical point of view, one-bit sampling is done efficiently at a very high rate with a significantly lower cost compared to its high-resolution counterpart. Thus, by employing one-bit ADCs,

III. ONE-BIT PHASE RETRIEVAL WITH SAMPLE ABUNDANCE

As indicated earlier, employing one-bit quantization provides a practical opportunity to address an important question as to whether more samples can mean less complexity in the context of the phase retrieval problem. We begin our efforts by defining a linear system of inequalities representing the phase retrieval problem in the one-bit quantization system deploying time-varying thresholds leading to the *one-bit phase retrieval* formulation. To recover the desired symmetric positive semi-definite matrix X^* , we propose an algorithm which relies on exploiting the large number of one-bit sampled data and solves the associated linear system of inequalities by taking advantage of *the randomized Kaczmarz algorithm* (RKA).

A. Problem Formulation

In the one-bit sampling scenario, we only observe sign data r, given as

$$r = \operatorname{sgn}(\mathbf{y} - \boldsymbol{\tau}), \tag{7}$$

where τ is a time-varying¹ threshold. Let e denote the phase vector to be recovered. The one-bit phase retrieval problem can be formulated as:

find
$$\mathbf{y}, \mathbf{x}, \mathbf{e}$$

 $\mathbf{y} \odot \mathbf{e} = A\mathbf{x},$
 $\mathbf{y} \in \Psi,$
(8)

where Ψ is a feasible region created by the one-bit constraints

$$r_i(y_i - \tau_i) \ge 0, \quad j \in \mathcal{J},$$
 (9)

or equivalently,

$$\Omega\left(\mathbf{v}-\boldsymbol{\tau}\right) \succeq 0,\tag{10}$$

with the matrix Ω defined as $\Omega = \operatorname{diag}\{r\}$. Inspired by (8), in the following, we present a reformulation of the one-bit phase retrieval problem. Since $y_j \geq 0$ based on (3), assuming $\tau_j \geq 0$, the following relation holds:

$$y_j \leq \tau_j \Longleftrightarrow y_i^2 \leq \tau_i^2.$$
 (11)

Therefore, the set of inequalities in (9) can be rewritten as

$$r_j(y_j - \tau_j) \ge 0 \Longrightarrow r_j(y_j^2 - \tau_j^2) \ge 0, \quad j \in \mathcal{J}.$$
 (12)

Consequently, one can recast (8) in the same spirit as (5):

find
$$X$$

s.t. $r_{j} \left(\operatorname{Tr} \left(V_{j} X \right) - \tau_{j}^{2} \right) \geq 0,$
 $\operatorname{rank} \left(X \right) = 1,$
 $X \succeq 0.$ (13)

Moreover, based on (6), the one-bit version of the PhaseLift formulation may be written as

$$\min_{\boldsymbol{X}} \quad \operatorname{Tr}(\boldsymbol{X})$$
s.t. $r_{j} \left(\operatorname{Tr}(\boldsymbol{V}_{j}\boldsymbol{X}) - \tau_{j}^{2} \right) \geq 0,$ (14)
$$\boldsymbol{X} \succeq 0,$$

3

which we refer to as *one-bit PhaseLift* in this paper. It is worth noting that the problem in (14) also belongs to the class of semi-definite programs (SDPs). As discussed earlier, in the asymptotic case of the one-bit phase retrieval problem, the PSD constraint may not be required. Moreover, the linear system of inequalities in (14) can be reformulated as

$$\operatorname{Tr}(V_{j}X) = \operatorname{vec}(V_{j}^{\top})^{\top} \operatorname{vec}(X), \quad j \in \mathcal{J},$$
 (15)

where we use the matrix identity [38],

$$\operatorname{Tr}(\boldsymbol{H}^{\top}\boldsymbol{D}) = \operatorname{vec}(\boldsymbol{H})^{\top}\operatorname{vec}(\boldsymbol{D}), \tag{16}$$

with H and D being two arbitrary square matrices. As a result, the constraints imposed in the optimization problem (14) can be simplified as

$$\min_{\boldsymbol{X}} \quad \operatorname{Tr}(\boldsymbol{X}) \\
\text{s.t.} \quad (\boldsymbol{R} \odot \boldsymbol{V}) \operatorname{vec}(\boldsymbol{X}) \succeq \boldsymbol{r} \odot \boldsymbol{\tau}^{2}, \tag{17}$$

where $R = \mathbf{1}_{n^2}^{\top} \otimes r$, and V is a matrix with $\text{vec}\left(V_j^{\top}\right)^{\top}$ as its j-th row $(j \in \mathcal{J})$.

Note that dropping the PSD constraint is not the only advantage of having access to a large number of one-bit sampled data in the context of phase retrieval problem. In fact, we claim that by our approach the rank-one, or its relaxed versions potentially manifested as a trace minimization, also become redundant. To see why, observe that in the asymptotic case of one-bit phase retrieval, the space constrained by the defined inequalities in (12), which is a polyhedron, *shrinks* to become contained inside the feasible region in terms of the PSD constraint. However, this shrinking space always contains the globally optimal rank-one solution, with a volume that is decreasing with an increasing number of samples. Thus, instead of the optimization problems in (14) and (17), we formally define the said polyhedron, i.e.,

$$\mathcal{P} = \left\{ \boldsymbol{X} \mid r_j \left(\text{Tr} \left(\boldsymbol{V}_j \boldsymbol{X} \right) - \tau_j^2 \right) \ge 0, \quad j \in \mathcal{J} \right\}, \quad (18)$$

equivalently restated based on (15) as

$$\mathcal{P} = \left\{ \boldsymbol{X} \mid r_{j} \operatorname{vec} \left(\boldsymbol{V}_{j}^{\top}\right)^{\top} \operatorname{vec} \left(\boldsymbol{X}\right) \geq r_{j} \tau_{j}^{2}, \quad j \in \mathcal{J} \right\}. \tag{19}$$

A numerical investigation of (19) reveals that by increasing the number of samples m, the space formed by the intersection of half-spaces (inequality constraints) can fully shrink to the optimal point inside the PSD constraint—see Fig. 1 for an illustrative example of this phenomenon. As can be seen in this figure, the black lines representing the linear inequalities form a finite-volume space around the optimal point displayed by the purple circle inside the PSD cone (the elliptical region²) by growing the number of one-bit samples. In (a)/(d), constraints

¹Note that although we are focusing on temporal sampling, the low cost associated with one-bit ADCs enables the deployment of large arrays of ADCs that are spatially distributed, which is of immediate use in various communications and imaging applications. This paves the way for spatially-varying sampling thresholds, possibly along with time-varying thresholds. Fortunately, the mathematical foundations and algorithms we present in this work can be directly applied to cases where spatially-varying thresholds are used as well.

²Note that a two-dimensional slice of the three-dimensional PSD cone typically assumes an elliptical form.

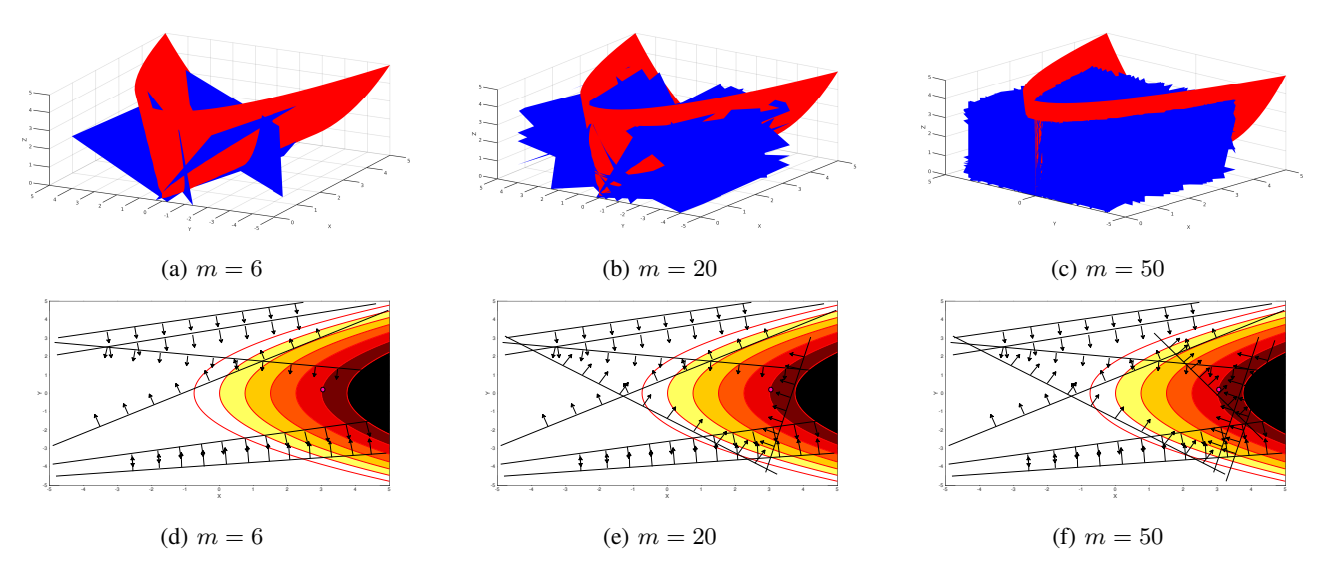


Figure 1: Shrinkage of the polyhedron space (19), ultimately placed within the PSD cone $X \succeq 0$ shown with contours and its red boundary, when the number constraints (samples) grows large. The arrows point to the half-space associated with each inequality constraint. The evolution of the feasible regime is depicted with increasing samples in three cases: (a) and (d) small sample-size regime, constraints not forming a finite-volume polyhedron; (b) and (e) medium sample-size regime, constraints forming a finite-volume polyhedron, parts of which are outside the cone; (c) and (f) large sample-size regime, constraints forming a finite-volume polyhedron inside the PSD cone, making the PSD constraint redundant. The optimal point representing the signal to be recovered is shown by purple.

are not enough to create a finite-volume space, whereas in (b)/(e) such constraints can create the desired finite-volume polyhedron space which, however, is not fully inside the PSD cone. Lastly, in (c)/(f), the created finite-volume space shrinks to be fully inside the PSD cone.

To find the signal of interest in the polyhedron (19), we use the RKA without enforcing other costly constraints. This is due to the fact that the solution may be efficiently approached by solving the linear system of inequalities presented in (19).

Note that two signal models for the phase retrieval problem were introduced in [11]: (1) The real-valued model: the unknown signal \mathbf{x} and $\{a_j\}$ are real. (2) The complex-valued model: the unknown signal \mathbf{x} and $\{a_j\}$ are complex [11]. Both settings will be considered in the following proposed algorithm.

B. One-Bit Phase Retrieval Algorithm (OPeRA)

To recover the desired signal in the one-bit phase retrieval problem, we aim to find a point in the polyhedron (19) instead of solving the SDP in (6). As discussed in Section III-A, when we exploit a large number of samples, the solution of (19) is increasingly likely to capture the desired point, i.e. the signal of interest, inside the PSD conical region. The proposed signal recovery relies on the RKA, which is a powerful tool for solving real- or complex-valued linear system of equations, or inequalities through projections [39], [40].

Accordingly, we propose an algorithm to find the desired matrix X^* in (13) by (i) using abundant measurements, in order to create the finite-volume space inside the PSD conical region (discussed further in Section IV), and (ii) solving (19) via the RKA. We name our algorithm the *One-bit Phase Retrieval Algorithm* (OPeRA).

The RKA is a sub-conjugate gradient method to solve overdetermined linear systems, i.e, $C\mathbf{x} \leq \mathbf{b}$ where C is a $m \times n$ matrix with m > n [40], [41]. Conjugate-gradient methods immediately turn the mentioned inequality to an equality in the following form:

$$\left(\mathbf{C}\mathbf{x} - \mathbf{b}\right)^{+} = 0,\tag{20}$$

and then, approach the solution by the same process as used for systems of equations. Without loss of generality, consider (20) to be a polyhedron:

$$\begin{cases} \mathbf{c}_{j}\mathbf{x} \leq b_{j} & (j \in I_{\leq}), \\ \mathbf{c}_{j}\mathbf{x} = b_{j} & (j \in I_{=}), \end{cases}$$
 (21)

where the disjoint index sets I_{\leq} and $I_{=}$ partition our sample index set \mathcal{J} , and $\{c_j\}$ denote the rows of C. Based on this problem, the projection coefficient β_i of the RKA is defined as [39], [40], [42]:

$$\beta_i = \begin{cases} (\boldsymbol{c}_j \mathbf{x}_i - b_j)^+ & (j \in I_{\leq}), \\ \boldsymbol{c}_j \mathbf{x}_i - b_j & (j \in I_{=}). \end{cases}$$
 (22)

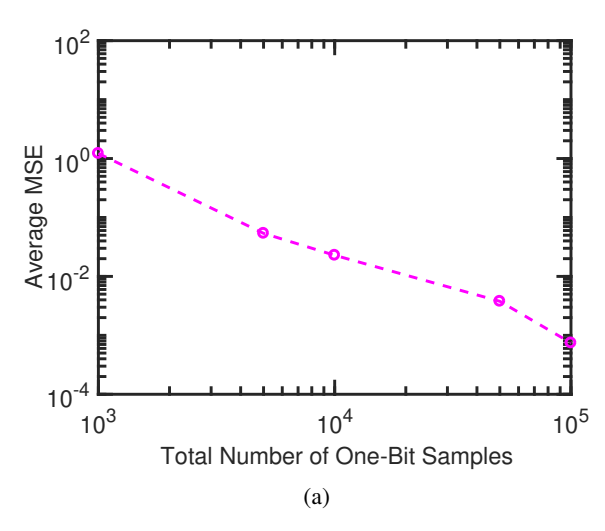
Also, the unknown column vector \mathbf{x} is iteratively updated as:

$$\mathbf{x}_{i+1} = \mathbf{x}_i - \frac{\beta_i}{\|\mathbf{c}_j\|_2^2} \mathbf{c}_j^{\mathrm{H}},\tag{23}$$

where, at each iteration i, the index j is chosen independently at random from the set \mathcal{J} , following the distribution

$$P\{j=k\} = \frac{\|\boldsymbol{c}_k\|_2^2}{\|\boldsymbol{C}\|_{\mathrm{F}}^2}.$$
 (24)

To ensure a limited error, the feasible region in (19) cannot be an infinite space in an asymptotic sense. Fortunately, by



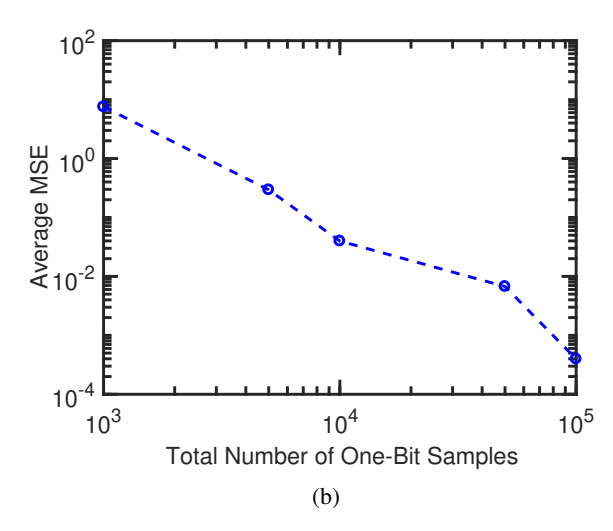


Figure 2: Average MSE for signal recovery (in terms of spectral radius of X) for different one-bit sample sizes with OPeRA: (a) $\mathbf{x} \in \mathbb{R}^n$, (b) $\mathbf{x} \in \mathbb{C}^n$.

introducing more samples, the problem can form a polyhedron with a bounded volume containing the desired point. Even more interesting, by adding more inequality constraints in (19), the shrinkage of the said polyhedron will put a downward pressure on the error between the desired and recovered points (each informative sample will shrink this space). We will show that by increasing the number of constraints and effective sampling, this error approaches zero. Moreover, as a result of using an overdetermined linear system of inequalities, the convergence of the RKA is guaranteed [39], [40].

It is worth noting that, in our problem, we only have the inequality partition I_{\leq} . Herein, the row vectors $\{\boldsymbol{c}_j\}$ and the scalars $\{b_j\}$ used in the RKA (21)-(24) are $-\left\{r_j\operatorname{vec}\left(\boldsymbol{V}_j^{\top}\right)^{\top}\right\}$ and $-\left\{r_j\tau_j^2\right\}$, respectively.

C. Numerical Illustrations for OPeRA

We numerically examine the effect of growing the sample size in the recovery of the desired matrix X^* in OPeRA. We will use the spectral radius metric which is particularly informative in the recovery of rank-one matrices. Note that for a positive semi-definite matrix such as our desired matrix X^* , the spectral radius is equal to the Frobenius norm of the matrix [38]. In all experiments, the input signals were generated as $\mathbf{x} \sim \mathcal{N}(\mathbf{0}, I_n) + j\mathcal{N}(\mathbf{0}, I_n)$ for the complex-valued model, and $\mathbf{x} \sim \mathcal{N}(\mathbf{0}, I_n)$, for the real-valued model. The rows of the sensing matrix A were generated as $a_j \sim \mathcal{N}(\mathbf{0}, I_n) + j\mathcal{N}(\mathbf{0}, I_n)$ for complex-valued model, and $a_j \sim \mathcal{N}(\mathbf{0}, I_n)$, for the real-valued model. Accordingly, we made use of the time-varying thresholds $\tau \sim \text{Lognormal}(0, 1)$. We define the experimental mean square error (MSE) between the true spectral radius $\rho(X)$ and its estimate $\rho(\bar{X})$ as

$$MSE \triangleq \frac{1}{E} \sum_{e=1}^{E} \left| \rho_e \left(\mathbf{X}^* \right) - \rho_e \left(\bar{\mathbf{X}} \right) \right|^2, \tag{25}$$

where E is the number of experiments. Each presented data point is averaged over 10 experiments. The re-

Table I: Average NMSE for OPeRA with different signal dimensions.

OPeRA	n = 30	n = 50	n = 128
NMSE	4.3359e-08	3.9485e-08	2.1566e-07
m^{\star}	3000	8000	20000

sults are obtained for the number of samples $m \in \{1000, 5000, 10000, 50000, 100000\}$.

Fig. 2 appears to confirm the possibility of recovering the spectral radius of X^* from the large number of one-bit sampled data with time-varying thresholds by OPeRA for the real-valued and the complex-valued models, respectively. As expected, the performance of the recovery will be significantly enhanced as the number of one-bit samples grows large. In all experiments, the obtained maximum eigenvalue is positive, which is equal to the spectral radius of the recovered matrix.

An important part of our work is to show that our method can recover an X that is "increasingly" rank-one and PSD by growing the number of one-bit sampled data. To do so, at first, we show in Fig. 2 that the maximum eigenvalue is accurately recovered. Next, we present that all eigenvalues $\{\ell_i\}$ of the recovered matrix \bar{X} except the maximum eigenvalue approach zero by increasing the number of one-bit sampled data. Fig. 3 appears to confirm this claim for both real-valued and complex-valued models. The presented results are averaged over 10 experiments and the eigenvalues are arranged in descending order.

To further investigate the effectiveness of OPeRA in both real-valued and complex-valued models, Fig. 4 illustrates the squared Frobenius norm of the error normalized by the squared Frobenius norm of the desired matrix X^* , defined as

$$NMSE \triangleq \frac{\left\| \boldsymbol{X}^* - \bar{\boldsymbol{X}} \right\|_{F}^{2}}{\left\| \boldsymbol{X}^* \right\|_{F}^{2}}, \tag{26}$$

where the presented results are averaged over 10 experiments. Fig. 4 appears to confirm that the performance of the recovery is enhanced by increasing the number of one-bit samples.

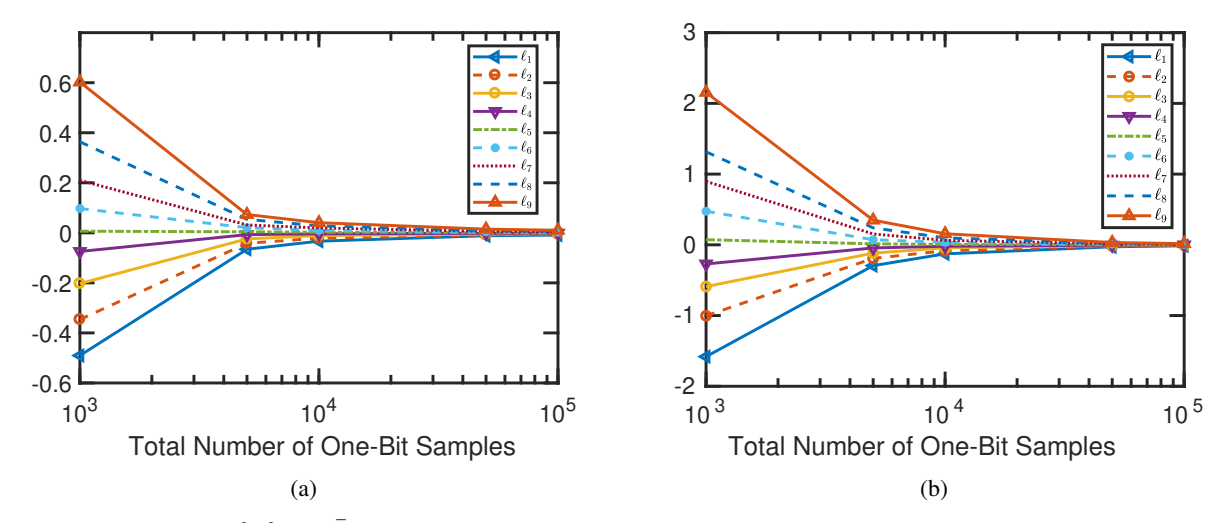


Figure 3: The eigenvalues $\{\ell_i\}$ of \bar{X} (excluding the maximum eigenvalue) averaged over 10 experiments: (a) $\mathbf{x} \in \mathbb{R}^n$, (b) $\mathbf{x} \in \mathbb{C}^n$. Deploying a large number of samples leads to obtaining an X that is "increasingly" rank-one PSD.

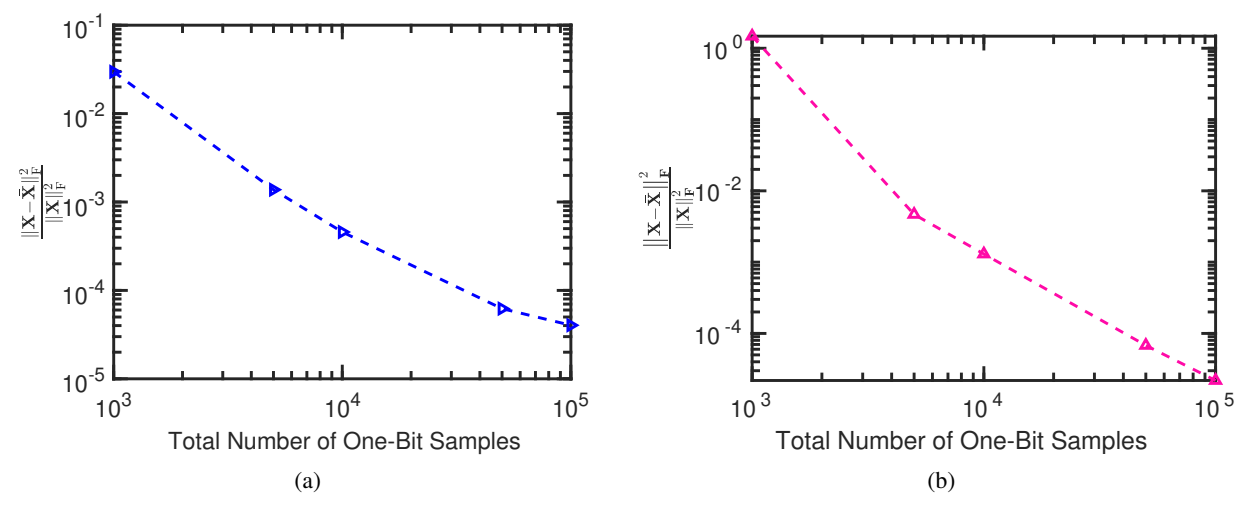


Figure 4: Average NMSE for the Frobenius norm error between the desired matrix X^* and its recovered version \bar{X} for different one-bit sample sizes with the RKA applied to (19) when (a) $\mathbf{x} \in \mathbb{R}^n$, (b) $\mathbf{x} \in \mathbb{C}^n$.

The main difference of reported results of real and complex domains is that we have to increase the number of iterations in RKA for the recovery of complex signals, because of their more complexity compared to that of signals in the real domain.

To examine the performance of OPeRA for moderate and high dimensional input signals, we consider input signals with dimensions $n \in \{30, 50, 128\}$ which their results are averaged over 15 experiments and reported in Table I. As can be seen, our proposed recovery method appears to perform well in high dimensional scenario. These results are obtained by using the random time-varying sampling thresholds which are chosen to be close to the measurements $\{y_j\}$; i.e., $\tau = \mathbf{y} + \boldsymbol{\epsilon}$, where $\boldsymbol{\epsilon}$ is a normal random vector $\boldsymbol{\epsilon} \sim \mathcal{N}\left(\mathbf{0}, 0.02\boldsymbol{I}\right)$.

IV. BOUNDING THE RECOVERY ERROR

In this section, we derive the convergence rate of our proposed algorithm in its search for the optimal point in the PSD cone. Moreover, an upper bound for the recovery error $\mathbb{E}\left\{\left\|X_i-X^\star\right\|_{\mathrm{F}}^2\right\}$ will be introduced. This bound will be leveraged to find a lower bound on the number of measurements m; the critical role of which was readily discussed in Section III.

A. Chernoff Bound Analysis for OPeRA

We first investigate the convergence of OPeRA through a probabilistic lens. Define the distance between the optimal point X^* and the j-th hyperplane presented in (19) as

$$H_{j}\left(\boldsymbol{X}^{\star}, \boldsymbol{X}_{i}\right) = \left|\operatorname{Tr}\left(\boldsymbol{V}_{j} \boldsymbol{X}_{i}\right) - \operatorname{Tr}\left(\boldsymbol{V}_{j} \boldsymbol{X}^{\star}\right)\right|,$$

$$= \left|\operatorname{Tr}\left(\boldsymbol{V}_{i}\left(\boldsymbol{X}_{i} - \boldsymbol{X}^{\star}\right)\right)\right|, \quad j \in \mathcal{J},$$
(27)

where X_i is the solution from the RKA iterations. From an intuitive point of view, it is easy to observe that by generally reducing the distances between X^* and the constraint-associated hyperplanes, the possibility of *capturing* the optimal point is increased.

Suppose $\mathcal K$ is the cardinality of the set of the hyperplanes presented in (19), a portion of the whole sample size, i.e., $\mathcal K \leq m$, which will effectively form a polyhedron inside the PSD cone around the optimal point $\boldsymbol X^\star$ if the number of samples is sufficient. The average of the distances $\{H_j\}$ around the optimal point is obtained as

$$\mathcal{E}\left(\boldsymbol{X}^{\star}\right) = \frac{1}{\mathcal{K}} \sum_{j=1}^{\mathcal{K}} H_{j}\left(\boldsymbol{X}^{\star}, \boldsymbol{X}_{i}\right), \quad \mathcal{K} \subseteq \mathcal{J}.$$
 (28)

For a specific sample size m, when the area of the finite-volume space around the optimal point is reduced, $\mathcal{E}\left(\boldsymbol{X}^{\star}\right)$ is diminished as well. Define the overall average distance T_{ave} as

$$T_{\text{ave}} = \frac{1}{m} \sum_{j=1}^{m} H_j \left(\boldsymbol{X}^*, \boldsymbol{X}_i \right), \quad m \in \mathcal{J}.$$
 (29)

Increasing the number of samples leads to smaller values of $\mathcal{E}\left(\boldsymbol{X}^{\star}\right)$ and T_{ave} . Therefore, the possibility of creating the finite-volume space around the desired point increases in the asymptotic sample-size scenario, with $m \geq m^{\star}$, where m^{\star} is the minimal measurement size. The *Chernoff Bound* [43], [44] can shed light on this phenomenon as illustrated bellow.

Theorem 1. Consider the distances $\{H_j(\mathbf{X}^*, \mathbf{X}_i)\}$ between the desired point \mathbf{X}^* and the hyperplanes of the polyhedron defined in (19) to be i.i.d. random variables.

• The Chernoff bound of T_{ave} in (29) is given by

$$\Pr\left(T_{ave} = \frac{1}{m} \sum_{j=1}^{m} H_j\left(\boldsymbol{X}^{\star}, \boldsymbol{X}_i\right) \le a\right) \ge 1 - \inf_{t \ge 0} \frac{M_T}{e^{ta}},$$
(30)

where M_T is the moment generating function (MGF) of T_{ave} , given as

$$M_{T} = \left(1 + t \frac{\mu_{H_{j}}^{(1)}}{m} + \dots + t^{\kappa} \frac{\mu_{H_{j}}^{(\kappa)}}{\kappa! \, m^{\kappa}} + \mathcal{R}\left(m\right)\right)^{m},$$
(31)

with $\mu_{H_j}^{(\kappa)} = \mathbb{E}\{H_j^{\kappa}\}$, and \mathcal{R} denoting a bounded remainder associated with truncating the Taylor series expansion of M_T .

 M_T is decreasing with an increasing sample size in the sample abundance scenario, leading to an increasing lower bound in (30).

Proof. The MGF of T_{ave} is given by

$$M_T = \mathbb{E}\left\{e^{t\frac{1}{m}\sum_{j=1}^m H_j}\right\} = \prod_{j=1}^m \mathbb{E}\left\{e^{t\frac{H_j}{m}}\right\}$$
$$= \mathbb{E}\left\{e^{t\frac{H_j}{m}}\right\}^m.$$
 (32)

By using the Taylor series expansion, one can write

$$M_T = \mathbb{E}\left\{1 + t\frac{H_j}{m} + t^2\frac{H_j^2}{2m^2} + t^3\frac{H_j^3}{6m^3} + \cdots\right\}^m,$$
 (33)

which leads to the formulation (31). Note that due to the fact that the distances $\{H_j\}$ can be considered to be finite values, their moments always exist.

It is straightforward to verify that M_T is an analytic function and that $|\mathcal{R}(m^*)|$ is bounded. Let t_0 denote the value of t making the upper bound in (30) infimum. To prove that M_T is a decreasing function in the asymptotic sample-size case $(m>m^*)$, we use the Padé approximation (PA) which can asymptotically approximate M_T with a rational function of given order through the *moment matching* technique as follows [24], [28], [29]:

$$\forall m > m^*: M_T = \left(1 + \dots + t_0^{\kappa} \frac{\mu_{H_j}^{(\kappa)}}{\kappa! \, m^{\kappa}}\right)^m \approx \frac{a_0 + \frac{a_1}{m}}{b_0 + \frac{b_1}{m}},$$
(34)

where $\{a_0, a_1, b_0, b_1\}$ are the PA coefficients as given in [24]. The above rational approximation³ is a decreasing function; a fact that can be verified by taking its first derivative with respect to m. The negativity of the derivative is easily concluded by observing that

$$\sigma_{H_j}^2 = \mu_{H_j}^{(2)} - \left(\mu_{H_j}^{(1)}\right)^2 \ge 0,$$
 (35)

where $\sigma_{H_j}^2$ is the non-negative variance of the random variable H_j .

B. Recovery Error Upper Bound for OPeRA

In order to find the signal of interest in the polyhedron (19), we are utilizing the RKA which its convergence rate obtained as the following lemma.

Lemma 1 (See [40], [41]). RKA converges linearly in expectation:

$$\mathbb{E}\left\{\left\|\mathbf{x}_{i}-\mathbf{x}^{\star}\right\|_{2}^{2}\right\} \leq q^{i}\left\|\mathbf{x}_{0}-\mathbf{x}^{\star}\right\|_{2}^{2},\tag{36}$$

where \mathbf{x}^* is a desired point, $q \in (0,1)$ is a function of the condition number of the matrix \mathbf{C} , and i is the number of required iterations for the RKA.

In our problem, $\mathbf{x}_i = \text{vec}(\mathbf{X}_i)$, $\mathbf{x}^* = \text{vec}(\mathbf{X}^*)$, and $\mathbf{C} = \mathbf{R} \odot \mathbf{V}$. Therefore, the left-hand side of (36) may be recast as

$$\mathbb{E}\left\{\left\|\operatorname{vec}\left(\boldsymbol{X}_{i}\right)-\operatorname{vec}\left(\boldsymbol{X}^{\star}\right)\right\|_{2}^{2}\right\}=\mathbb{E}\left\{\left\|\boldsymbol{X}_{i}-\boldsymbol{X}^{\star}\right\|_{\mathrm{F}}^{2}\right\}.$$
 (37)

It is clear from (36) that by using a well-chosen initial point \mathbf{x}_0 or by increasing the number of iterations i, the recovery error can be further contained. Nevertheless, in the proposed recovery approach, it is deemed necessary to have the sufficient number of samples (inequalities) in order to guarantee a finite-volume feasible region and a bounded recovery error. Once our search area is located inside the PSD cone, we may effectively employ (36) for the convergence rate. The convergence rate of the RKA is useful when we have a linear system of inequalities. On the other hand, in the one-bit phase retrieval, the main constraints, i.e. the rank-one and the PSD, are non-linear and they may be considered to be redundant by deploying the enough number of samples. Thus, (36) is insufficient to present the convergence rate of OPeRA. We

³Considering the Taylor series expansion of M_T , the PA with the utilized orders presented in (34) will approximate M_T with an error in the order of $\mathcal{O}(m^{-3})$ for $m>m^*$.

can make (36) relevant to the one-bit phase retrieval problem by taking a penalty function into consideration:

$$\mathbb{E}\left\{\left\|\boldsymbol{X}_{i}-\boldsymbol{X}^{\star}\right\|_{\mathrm{F}}^{2}\right\} \leq q^{i}\left\|\boldsymbol{X}_{0}-\boldsymbol{X}^{\star}\right\|_{\mathrm{F}}^{2}+\Psi\left(m\right),\tag{38}$$

where $\Psi(.)$ is a decreasing function in the abundance samplesize regime, such that if the number of samples is enough to satisfy the PSD constraint, the penalty function approaches zero $\Psi\left(m\right)\to0$. Based on our discussion in Section IV-A, a good example for $\Psi\left(m\right)$ can be $M_{T}-M_{\infty}$, where $M_{\infty}=\lim_{m\to\infty}M_{T}$.

To find a bound for the sufficient number of measurements m to create a finite-volume space inside the PSD cone and the penalty function starts to be zero, we utilize the tail function of the penalty given by

$$\Psi^{\star}(m) = \Psi(m)\mathbb{I}_{(m > m^{\star})}. \tag{39}$$

Tails of decreasing functions may be asymptotically approximated by an exponential function [44]. Mathematically, this may be expressed as

$$\exists \epsilon_0, \gamma_1 \in \mathbb{R}^+, \quad \sup_{m} \left| \Psi^*(m) - \epsilon_0 e^{-\gamma_1 m} \right| < \varepsilon,$$
 (40)

where ε is an arbitrarily small positive number. To evaluate ϵ_0 and γ_1 , we can utilize the PA of $\Psi\left(m\right)=M_T-M_\infty$ defined in (34) as follows:

$$\epsilon_0 e^{-\gamma_1 m_1} = \frac{a_0 + \frac{a_1}{m_1}}{b_0 + \frac{b_1}{m_1}} - \frac{a_0}{b_0},$$

$$\epsilon_0 e^{-\gamma_1 m_2} = \frac{a_0 + \frac{a_1}{m_2}}{b_0 + \frac{b_1}{m_2}} - \frac{a_0}{b_0},$$
(41)

where $m_1 = m^*$, $m_2 = Cm^*$, and C is chosen to be a large positive number. Consequently, ϵ_0 and γ_1 are given by

$$\gamma_1 = \frac{1}{m_2 - m_1} \ln \left(\frac{f_p(m_1)}{f_p(m_2)} \right),$$

$$\epsilon_0 = f_p(m_1) e^{\gamma_1 m_1},$$
(42)

where $f_p(m)=rac{a_0+rac{a_1}{m}}{b_0+rac{b_1}{m}}-rac{a_0}{b_0}$. Note that $f_p(m)$ is the decreasing function and $rac{f_p(m_1)}{f_p(m_2)}\geq 1$. By using (41), we formulate the exponential function

By using $(41)^{p}$ we formulate the exponential function $\epsilon_0 e^{-\gamma_1 m_1}$ in such a way to follow the penalty function in the beginning point m^* , and its tails behavior. Therefore, the boundary (38) is reformulated for $m \geq m^*$ as

$$\mathbb{E}\left\{\left\|\boldsymbol{X}_{i}-\boldsymbol{X}^{\star}\right\|_{\mathrm{F}}^{2}\right\} \leq q^{i}\left\|\boldsymbol{X}_{0}-\boldsymbol{X}^{\star}\right\|_{\mathrm{F}}^{2}+\epsilon_{0}e^{-\gamma_{1}m}.\tag{43}$$

C. Lower Bound on the Number of Measurements

The algorithm termination criterion is considered to be

$$\mathbb{E}\left\{\left\|\boldsymbol{X}_{i}-\boldsymbol{X}^{\star}\right\|_{\mathrm{F}}^{2}\right\} \leq \epsilon_{1}.\tag{44}$$

Based on this criterion and (43), the following theorem is presented in order to find a lower bound for the number of required measurements in OPeRA.

Theorem 2. To recover the desired PSD matrix X^* in accordance to (44) in one-bit phase retrieval by OPeRA with

a probability of at least $1 - \inf\{M_T e^{-at}\}$, the number of measurements m must obey

$$m \ge \frac{1}{\gamma_1} \ln \left(\frac{\epsilon_0}{\epsilon_1 - q^i \omega_0} \right),$$
 (45)

where ϵ_0 and γ_1 are determined via (42), $\omega_0 = \|\mathbf{X}_0 - \mathbf{X}^{\star}\|_{\mathrm{F}}^2$ is the initial squared-error, and i is the number of iterations.

Proof. To satisfy (44), the inequality in (43) is adjusted to capture the upper bound ϵ_1 . As a result, the following inequality is obtained:

$$q^{i} \| \boldsymbol{X}_{0} - \boldsymbol{X}^{\star} \|_{\mathrm{F}}^{2} + \epsilon_{0} e^{-\gamma_{1} m} \le \epsilon_{1}. \tag{46}$$

Note that ω_0 is a constant scalar that only depends on the initial and optimal signals. According to (43), we can write

$$e^{-\gamma_1 m} \le \frac{\epsilon_1 - q^i \omega_0}{\epsilon_0},\tag{47}$$

or equivalently,

$$m \ge \frac{1}{\gamma_1} \ln \left(\frac{\epsilon_0}{\epsilon_1 - q^i \omega_0} \right).$$
 (48)

which proves the theorem.

The sufficient number of measurements m is sought to create a finite-volume in the PSD cone $X \succeq 0$ for the input signal x with the size n. It is easy to verify that the dimension of the PSD cone is equal to $\frac{n^2+n}{2}$ in both real-valued and complex valued cases. The infimum number of the hyperplanes creating a finite-volume space in a n'-dimensional region is n'+1. Consequently, we can write:

$$\inf \mathcal{K} = \frac{n^2 + n}{2} + 1, \quad \mathcal{K} \subseteq \mathcal{J}. \tag{49}$$

Therefore, to form the finite-volume space, the sample size m must be lower bounded by $\inf \mathcal{K}$:

$$m \ge \left(\frac{n^2 + n}{2} + 1\right). \tag{50}$$

The above bound helps us to establish a clear connection between the sample size and the problem dimension. However, since the boundary in (45) is concerned with containing the error after a finite-volume is formed, it is asymptotically tighter than (50). Therefore, by satisfying (45), the lower bound in (50) is typically met as well. To achieve the accuracy ϵ_1 with OPeRA, the finite volume space must be created inside the cone. Thus, the chosen number of measurements m^* satisfying the inequality (43), can satisfy (48) as well, since to create a finite volume space, we need at least $\frac{n^2+n}{2}$ samples.

V. COMPLEXITY INVESTIGATION

We examine the computational cost associated with the use of more samples by comparing our approach (OPeRA) with the PhaseLift method, its one-bit extension (one-bit PhaseLift) as defined in (14) and Wirtinger flow (WirtFlow). This comparison is based on the required computational time for different sample sizes.

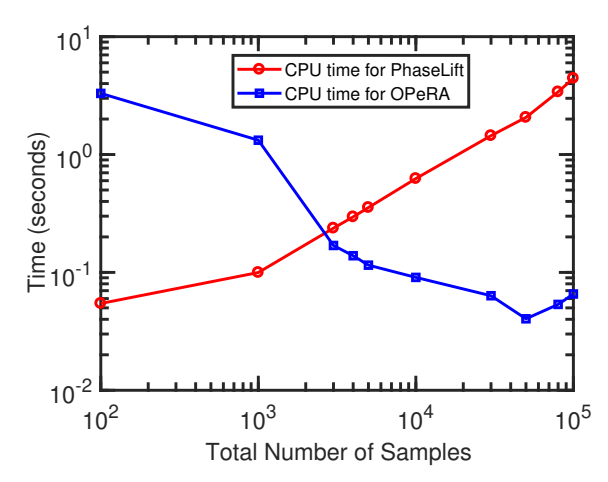


Figure 5: Comparing the PhaseLift method and OPeRA per CPU time when both methods use the stopping criterion $\mathbb{E}\left\{\|\boldsymbol{X}_i-\boldsymbol{X}^\star\|_{\mathrm{F}}^2\right\} \leq 10^{-2}$. Note that PhaseLift is applied to the high-resolution samples whereas only the one-bit version of the samples are made available to OPeRA.

A. Comparing PhaseLift and OPeRA

To compare the computational time for the SDP-based PhaseLift approach and our proposed method, the iterative algorithms are terminated according to (44) with $\epsilon_1=10^{-2}$. The unknown signal x lies within \mathbb{R}^{10} . The number of samples m is set to be 100, 1000, 3000, 4000, 5000, 10000, 30000, 50000, 80000, and 100000. Each CPU time is obtained by averaging over 5 experiments. PhaseLift is applied to the high-resolution samples, whereas OPeRA is applied to their one-bit sampled data counterpart, which means only partial information is made available to OPeRA.

As can be seen in Fig. 5, due to the growing number of samples, the cost of the PhaseLift algorithm has an increasing trend. Nevertheless, the CPU time for OPeRA experiences a significant decline rate from m=100 up until m=50000, while it starts increasing afterwards. The reason behind this behavior is hidden in the application of RKA. As discussed in Section IV, to create a finite-volume space around the optimal point X^* , and to capture error upper bound ϵ_1 , the number of samples has to move to the large-scale regimen. One may simply verify that, according to Theorem 2, by increasing the number of measurements m, the RKA may achieve the error upper bound with fewer iterations i. Additionally, the computational cost of the RKA used to solve (19) behaves as $\mathcal{O}(in^2)$. As a result, the CPU time for OPeRA may initially decrease with a growing number of samples.

Surpassing m=3000, the CPU time for OPeRA becomes smaller than that of the PhaseLift method; i.e. by employing sufficient number of samples, less complexity is achievable which is facilitated by dropping the PSD constraint. However, after approaching m=50000, we have increased the number of inequalities in such a way that the contribution to signal recovery is negligible, while at the same time, the extra measurements will still need processing. These extra inequalities may require more iterations to take them into

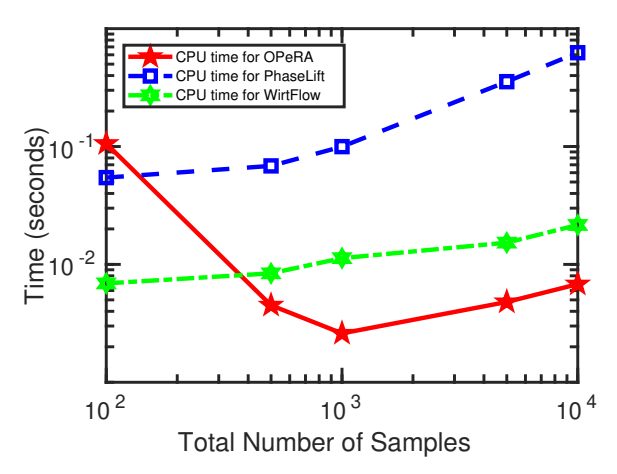


Figure 6: Comparing OPeRA, the PhaseLift method and the Wirtinger flow per CPU time when all methods use the stopping criterion $\mathbb{E}\left\{\|\boldsymbol{X}_i-\boldsymbol{X}^\star\|_{\mathrm{F}}^2\right\} \leq 10^{-2}$.

Table II: Comparing CPU times of the PhaseLift method, the Wirtinger flow and OPeRA with their optimal sample sizes.

Algorithm	m^{\star}	CPU time (s)
PhaseLift	30	0.0850
Wirtinger flow	30	0.0116
OPeRA	500	0.0045

account which is undesirable and increases the CPU time; see Fig. 5. Interestingly, OPeRA can satisfy the recovery criterion (44) with less CPU time and less input information compared to PhaseLift which is useful for the high-resolution scenario.

To further investigate the complexity of OPeRA, we compare it with that of the SDP and a popular local (non-convex) phase retrieval algorithm, the Wirtinger flow (WirtFlow) (see [14]) for different sample sizes in Fig. 6. In this comparison, we deploy the close time-varying thresholds to the measurements \mathbf{y} ; i.e., $\mathbf{\tau} = \mathbf{y} + \boldsymbol{\epsilon}$, where $\boldsymbol{\epsilon}$ is a normal random vector $\boldsymbol{\epsilon} \sim \mathcal{N}\left(\mathbf{0}, 0.02\mathbf{I}\right)$. As can be observed, after m=500, the performance of OPeRA has a lower CPU time compared to that of the SDP and the WirtFlow method. By comparing Fig. 5 and Fig. 6, one may conclude the importance of choosing time-varying sampling thresholds in OPeRA. When random thresholds are selected to be near the values of the measurements, they capture more information to use in the signal recovery which leads to employ less number of one-bit samples to achieve the termination criterion.

In Table II, CPU times of OPeRA, PhaseLift and WirtFlow methods are reported when the optimal number of samples are utilized where $m^\star = 3n\log n$ and $m^\star = 500$ are considered for high-resolution methods and OPeRA, respectively. Herein, optimal sample sizes mean the number of samples utilized by algorithms to show their best performance, i.e. the algorithm criterion $\|\boldsymbol{X}_i - \boldsymbol{X}^\star\|_F^2 \leq 10^{-4} \|\boldsymbol{X}^\star\|_F^2$. By this comparison, we remove the burden of the large number of samples from the SDP and the WirtFlow method to compare fairly their optimal shape deploying incomplete measurements, with OPeRA. As can be seen in Table II, OPeRA by using 500 one-bit samples

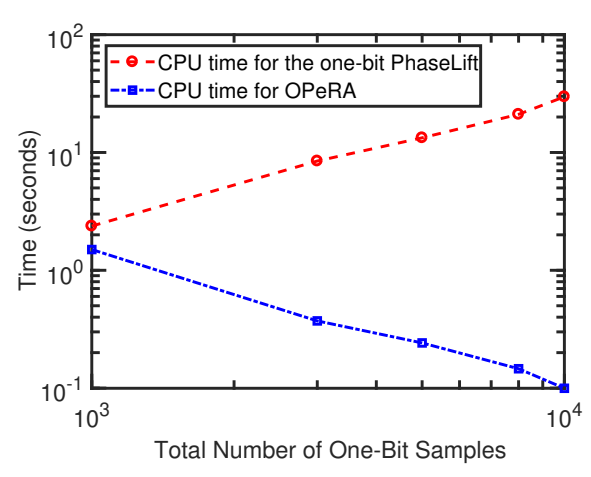


Figure 7: Comparing the one-bit PhaseLift method and OPeRA based on their CPU time when both algorithms are terminated using the criterion $\mathbb{E}\left\{\left\|\boldsymbol{X}_{i}-\boldsymbol{X}^{\star}\right\|_{\mathrm{F}}^{2}\right\}\leq10^{-2}$.

can recover the signal with the lower CPU time compared to that of the SDP and the WirtFlow method at which they are using incomplete measurements.

B. Comparing One-bit PhaseLift and OPeRA

Next, we compare the CPU time of the one-bit PhaseLift defined in (14) and that of OPeRA. As mentioned before, the one-bit PhaseLift problem is a SDP similar to the problem (6).

To compare the relaxation-based formulation of the onebit PhaseLift with our approach, we aim at the recovery of a signal $\mathbf{x} \in \mathbb{R}^{10}$ with sample sizes $m \in$ {1000, 3000, 5000, 8000, 10000}. The termination criterion of both algorithms is exactly similar to the one in Section V-A. As can be seen in Fig. 7, by growing the number of one-bit samples, the CPU time of the one-bit PhaseLift is increasing. On the other hand, the CPU time of OPeRA is decreasing. One may conclude that in the large sample size regimen, the proposed one-bit phase retrieval approach has a lower computational burden than one-bit PhaseLift. This due to enjoying the advantages of using more samples to make both the rank-one constraint and the PSD constraint redundant. We hypothesis that the computation time rise due to unhelpful extra samples (in achieving the error bound) occur well beyond m=10000, which is presumably why the increase is not observed in our experiment.

VI. ADAPTIVE TIME-VARYING THRESHOLDING

Hereafter, we propose an adaptive threshold design strategy for the task of one-bit phase retrieval. By the spirit of using the iterative RKA, a suitable time-varying threshold can be chosen in order to find the optimal solution with enhanced accuracy. As discussed earlier, with sample abundance, we have an overdetermined linear system of inequalities creating a finite-volume space. To capture the desired signal matrix X^* more efficiently, the right-hand side of the inequalities in (19), i.e. $r_j \tau_j^2$, must be determined in a way that each associated hyperplane passes through the desired feasible region within

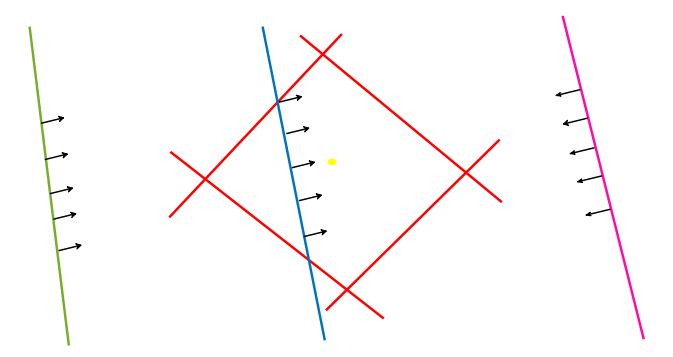


Figure 8: The signal of interest (shown by yellow circle) is located in the finite-volume space which presents itself as the red semi-rectangular. The new shrunken feasible region created by the blue hyperplane captures the desired signal. However, the other two sampling hyperplanes are non-informative.

the PSD cone. Therefore, an algorithm is proposed to ensure that this occurs. To give an illustration, we suppose the solution is the yellow point in Fig. 8. Geometrically, with an adaptive time-varying threshold algorithm, our goal is to generate an informative sampling threshold creating the inequality constraint corresponding to the hyperplane shown by the blue line.

Unlike the other two inequality constraints (hyperplanes illustrated by green and purple lines in Fig. 8), the blue hyperplane will further shrink the feasible region for signal recovery. From this viewpoint, the other hyperplanes (green and purple lines) constitute extra inequality constraints that are not informative. As discussed in Section V-A, such extra samples (the extra inequality constraints) only increase the computational burden of the phase retrieval task.

A. Adaptive Threshold Design for OPeRA

In light of previous discussion, to achieve a better recovery accuracy for a specific sample size m, one may use the idea of shrinking the space imposed by the set of inequalities in (19) around the optimal solution X^* . To make this happen, we propose an iterative algorithm generating an adaptive threshold to accurately obtain the desired solution. To diminish the area of the finite-volume space around the optimal point, we update the time-varying threshold as

$$\operatorname{Tr}\left(\boldsymbol{V}_{j}\boldsymbol{X}^{(k)}\right) - r_{j}^{(k)}\epsilon_{j}^{(k)} = \left(\tau_{j}^{(k+1)}\right)^{2}, \quad j \in \mathcal{J}, \quad (51)$$

where $\left\{\epsilon_j^{(k)}\right\}$ at the j-th element of a positive vector $\boldsymbol{\epsilon}^{(k)}$ in the k-th iteration. This updating process is based on the fact that when $r_j = +1$, we have $\operatorname{Tr}(\boldsymbol{V}_j\boldsymbol{X}) \geq (\tau_j)^2$, and $\operatorname{Tr}(\boldsymbol{V}_j\boldsymbol{X}) \leq (\tau_j)^2$ otherwise. The reason behind updating the one-bit measurements $\left\{r_j^{(k)}\right\}$, is to ensure that the optimal solution \boldsymbol{X}^* satisfies (19) in iteration k, i.e. the inequalities $r_j^{(k)} \operatorname{vec}(\boldsymbol{V}_j^\top)^\top \operatorname{vec}(\boldsymbol{X}^*) \geq r_j^{(k)} \left(\tau_j^{(k)}\right)^2$ for $j \in \mathcal{J}$. Our proposed iterative method to update the time-varying threshold is summarized in Algorithm 1.

B. Numerical Study of Adaptive Thresholding

To present the efficacy of the adaptive time-varying threshold algorithm in comparison with a non-negative random threshold, the unknown signal x and the sensing matrix A are generated using the same settings as in Section III-C. As can be seen in Fig. 9, the performance of our proposed algorithm is evaluated by the NMSE defined in (26) which is considerably enhanced in comparison with adopting a non-negative random threshold according to Lognormal (0, 1). The results are obtained for the sample sizes $m \in \{1000, 5000, 10000, 50000, 100000\}$ and $\delta = 10^{-3}$. Each presented data point is averaged over 5 experiments.

In the following, we compare the number of measurements m required to recover the rank-one and PSD matrix X^* using the OPeRA with (i) our proposed adaptive threshold algorithm, as well as (ii) a random non-negative threshold. The result can be summarized as follows.

Theorem 3. OPeRA with the adaptive sampling threshold proposed in Algorithm 1 can recover the rank-one and PSD matrix X^* with a high probability of at least $1-\inf\{M_Te^{-at}\}$ by using a smaller number of measurements m in comparison to OPeRA with a random threshold.

Proof. Let m_f denote the number of inequalities in (19) creating a finite-volume space around the desired matrix X^* , which is not necessarily inside the PSD cone. As discussed in Section VI-A, our proposed adaptive thresholding algorithm shrinks the finite-volume space around the optimal solution X^{\star} in a stronger way than the random thresholds. As a result, $\{H_j\}$ defined in (27) as well as their moments $\mu_{H_i}^{(k)}$, will further diminish which leads to a smaller value for M_T . Therefore, according to Theorem 1 and Theorem 2, a similar recovery performance can be expected with a smaller sample size when the adaptive sampling threshold proposed in Algorithm 1 is utilized. In other words, when time-varying sampling thresholds become closer to the measurements, their associated hyperplanes will be closer to the desired signal X^* . As a result, the volume of created finite space will further diminish as well. Therefore, due to the fact that the final solution of the RKA X_i is inside the created finite space, it gets closer to the desired point X^* , which leads to smaller distances $H_j(X^*, X_i)$, and subsequently smaller moments.

To numerically scrutinize our claim in Theorem 3, Table III illustrates that the sufficient number of samples m required for OPeRA to recover a PSD matrix with adaptive sampling thresholds proposed in Algorithm 1 is much less than that of OPeRA with a random threshold. The result is obtained for the input signal x, a random time-varying threshold τ , and the sensing matrix A originating from the same settings as presented in Section III-C. The number of samples examined in our experiments are same as Section V-A, plus m = 500.

To further investigate the effectiveness of Algorithm 1, we show that the average of all eigenvalues $\{\ell_i\}$ of X except the maximum eigenvalue (spectral radius) approaches zero by increasing the number of measurements—see Fig. 10. Algorithm 1 Adaptive Algorithm for Sampling Threshold Selection

Input: One-bit data: r, sensing matrix: A, initial timevarying thresholds: $\tau^{(0)} \sim \text{Lognormal}(0,1)$ (with the same length as r), small positive number: δ .

Output: Adaptive threshold: τ^* .

Note: $X^{(k)}$, $\tau^{(k)}$, $r^{(k)}$ and $\epsilon^{(k)}$ denote their associated values at iteration k.

- 1: Set $r^{(0)} = r$.
- 2: Calculate the matrix V with the rows $\{\text{vec}(a_i a_i^{\text{H}})^{\top}\}$.
- 3: Initiate the following loop by setting k=0. 4: **while** $\left\| m{ au}^{(k+1)} m{ au}^{(k)} \right\|_2 \leq \delta$ **do**
- Find a point inside the following polyhedron with the RKA for $\tau = \tau^{(k)}$:

$$\mathcal{P} = \left\{ \boldsymbol{X}^{(k)} \mid \left(\boldsymbol{R}^{(k)} \odot \boldsymbol{V} \right) \operatorname{vec} \left(\boldsymbol{X}^{(k)} \right) \geq \boldsymbol{b}^{(k)} \right\},$$

where $m{R}^{(k)}$ denotes the replica form of $m{r}^{(k)}$ and $m{b}^{(k)}=$

Update $\tau^{(k+1)}$ as:

$$m{r}^{(k)}\odot\left(m{ au}^{(k+1)}
ight)^2=\left(m{R}^{(k)}\odotm{V}
ight) ext{vec}\left(m{X}^{(k)}
ight)-rac{m{\epsilon}^{(k)}}{2},$$

where $\epsilon^{(k)}$ is computed as:

$$\boldsymbol{\epsilon}^{(k)} = \left(\boldsymbol{R}^{(k)} \odot \boldsymbol{V}\right) \operatorname{vec}\left(\boldsymbol{X}^{(k)}\right) - \boldsymbol{r}^{(k)} \odot \left(\boldsymbol{\tau}^{(k)}\right)^2.$$

- Update $r^{(k+1)}$ based on (12).
- Increase k by one.
- 9: end while

Table III: The number of samples required to recover a PSD

Proposed Algorithm	m
OPeRA with a random threshold	30000
OPeRA with the adaptive threshold	500

Interestingly, Fig. 10 reaffirms that the number of measurements used to recover the rank-one and PSD matrix X^* by OPeRA with adaptive thresholding, is much less than the same result reported in Fig. 3 where OPeRA with a random threshold is adopted. The results are obtained for the number of samples $m \in \{300, 500, 1000, 2000\}$, they are averaged over 5 experiments, and the non-dominant eigenvalues are arranged in a decreasing order.

It is worth noting that by considering the adaptive thresholding process in OPeRA, the overall complexity is $\mathcal{O}(kin^2)$, where k is the number of iterations in Algorithm 1, which is k=3 in our numerical results. For the results reported in Table III, the CPU time of OPeRA with the adaptive threshold is obtained as 0.0135 which is still less than that of the PhaseLift method reported in Table II, 0.0850.

VII. ONE-BIT PHASE RETRIEVAL WITH NOISY **MEASUREMENTS**

In this section, we extend our study to signal recovery from noisy one-bit data in the phase retrieval problem. In most

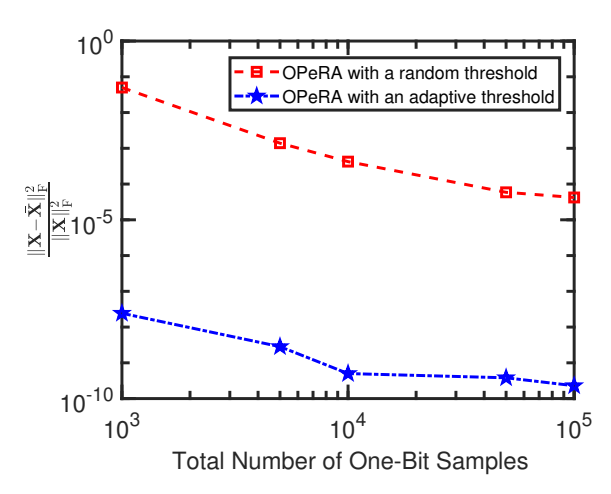


Figure 9: Comparing the average NMSE for the Frobenius norm between the desired matrix X^* and its recovered matrix using OPeRA when (i) a random threshold and (ii) the adaptive sampling threshold proposed in Algorithm 1, are adopted.

practical applications, we must rely on noisy measurements [23], [35], [45]. In particular, we will examine whether the computational advantages provided by sample abundance in the noiseless scenario will also be observed under the presence of noise.

A. Problem Formulation

Define the positive-valued vector $\boldsymbol{\mu} = [\mu_1, \cdots, \mu_m]$ by

$$\mu_j = \operatorname{Tr}(V_j X), \quad j \in \mathcal{J}.$$
 (52)

Let λ and z denote the time-varying threshold vector and the noise vector, respectively. The noisy one-bit samples are generated as

$$r_{j} = \begin{cases} +1 & \mu_{j} + z_{j} > \lambda_{j}, \\ -1 & \mu_{j} + z_{j} < \lambda_{j}. \end{cases}$$
 (53)

The occurrence probability vector p for the noisy one-bit measurement r is given as [45],

$$p_{j} = \begin{cases} \Phi(\mu_{j} - \lambda_{j}) & \text{for } \{r_{j} = +1\}, \\ 1 - \Phi(\mu_{j} - \lambda_{j}) & \text{for } \{r_{j} = -1\}, \end{cases}$$
 (54)

where $\Phi(.)$ is the CDF of $-\mathbf{z}$. Since $\{\mu_j\}$ are linear function of \boldsymbol{X} , the CDF of noise $\{\Phi(\mu_j-\lambda_j)\}$ can be written as $\Phi(\boldsymbol{X})$. The log-likelihood function of the sign data \boldsymbol{r} is given by

$$\mathcal{L}_{\boldsymbol{r}}(\boldsymbol{\mu}, \boldsymbol{X}) = \sum_{j=1}^{m} \left\{ \mathbb{I}_{(r_j = +1)} \log \left(\Phi(\mu_j - \lambda_j) \right) + \mathbb{I}_{(r_j = -1)} \log \left(1 - \Phi(\mu_j - \lambda_j) \right) \right\}.$$
(55)

Interestingly, by solving the maximum log-likelihood estimation (MLE) problem associated with (55), our desired matrix X^* can be immediately approximated. The proposed algorithm is called *Noisy OPeRA*.

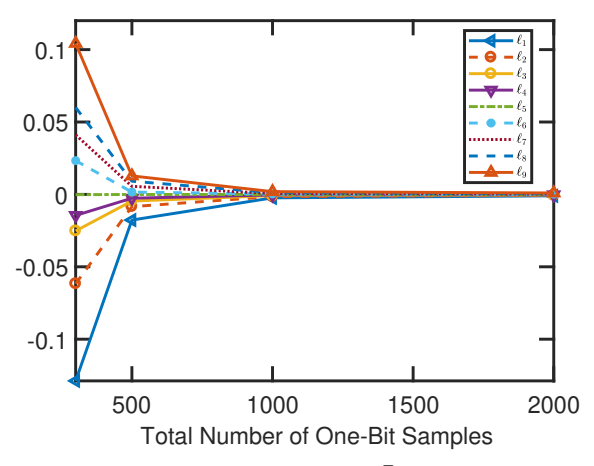


Figure 10: All eigenvalues $\{\ell_i\}$ of \bar{X} except the dominant eigenvalue (spectral radius), averaged over 5 experiments. As can be seen, deploying OPeRA with the adaptive sampling thresholds, leads to obtaining a nearly rank-one and PSD matrix with significantly enhanced accuracy as the number of samples grows large.

B. Noisy One-Bit Phase Retrieval via Convex Programming

A preliminary formulation of our optimization problem based on the MLE may be cast as:

$$\min_{\boldsymbol{\mu}, \boldsymbol{X}} \quad -\mathcal{L}_{\boldsymbol{r}}(\boldsymbol{\mu}, \boldsymbol{X})$$
s.t.
$$\mu_{j} = \operatorname{Tr}(\boldsymbol{V}_{j} \boldsymbol{X}), \quad j \in \mathcal{J},$$

$$\operatorname{rank}(\boldsymbol{X}) = 1,$$

$$\boldsymbol{X} \succeq 0.$$
(56)

This problem is the one-bit version of its counterpart formulated in [23]. However, as discussed in previous sections, because of employing one-bit sampling, the large number of samples can be adopted which leads to the availability of a large number of sign data $\{r_j\}$ and the corresponding inequality constraints; since when $r_j=+1$, we have ${\rm Tr}\,({\pmb V}_j{\pmb X}) \geq (\tau_j)^2$, and ${\rm Tr}\,({\pmb V}_j{\pmb X}) \leq (\tau_j)^2$ otherwise. These inequalities are collected to form the polyhedron (19). However, these constraints may be equivalently absorbed in the objective function to facilitate the one-bit phase retrieval formulation in the noisy case. Therefore, the problem (56) can be reformulated as

$$\min_{\boldsymbol{\mu}, \boldsymbol{X}} \quad -\mathcal{L}_{\boldsymbol{r}}(\boldsymbol{\mu}, \boldsymbol{X})
\text{s.t.} \quad \mu_{j} = \text{Tr}(\boldsymbol{V}_{j}\boldsymbol{X}), \quad j \in \mathcal{J}.$$
(57)

In many cases, $\mathcal{L}_{r}(\mu, \mathbf{X})$ is a concave function and thus the above programs becomes convex. One can readily verify this in the case of a Gaussian noise [35]. In the rest of our paper, $-\mathbf{z}$ is assumed to be an i.i.d. zero-mean Gaussian process $\mathbf{z} \sim \mathcal{N}\left(0, \sigma_{\mathbf{z}}^2 \mathbf{I}_m\right)$, for which $\Phi(.)$ is given in (1).

C. Numerical Investigation of Noisy OPeRA

To examine the performance of Noisy OPeRA in practice, and to validate the theoretical results described in this section, we consider signal recovery with different values of σ_z \in

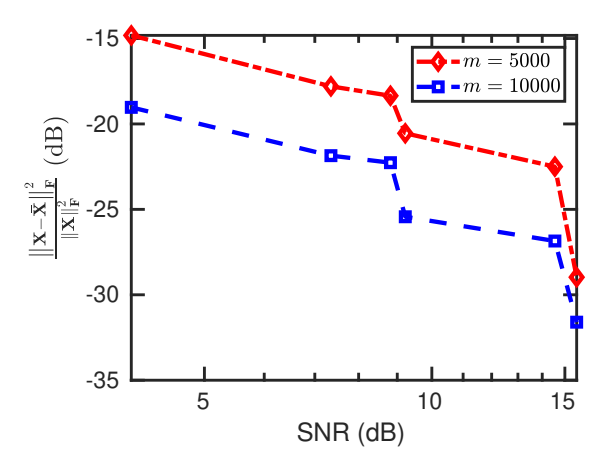


Figure 11: Average NMSE (dB) in the results obtained by the MLE problem (57) over different SNRs and for two different sample sizes $m \in \{5000, 10000\}$. It is observed that by increasing SNR and the number of one-bit measurements, the recovery performance of Noisy OPeRA is enhanced.

 $\{0.1, 0.2, 0.4, 0.5, 0.7, 1\}$, where the unknown signal \mathbf{x} was generated in a similar manner as in Section III-C. The stochastic threshold $\boldsymbol{\lambda}$ was generated according to $\boldsymbol{\lambda} \sim \mathcal{N}(0, I_m)$. The signal to noise ratio (SNR) is evaluated as:

$$SNR = \frac{\frac{1}{m} \sum_{j=1}^{m} \mu_j^2}{\sigma_{\mathbf{z}}^2}.$$
 (58)

In Fig. 11, the recovery performance is illustrated by using the NMSE defined in (26), with the results averaged over 10 experiments. We report both SNR and NMSE in dB ($10\log(.)$). As expected, by increasing the SNR, the performance of our method is improved. Furthermore, the performance of the estimation problem formulation in (57) is enhanced by increasing the number of one-bit samples $m \in \{5000, 10000\}$. In this approach, since the desired matrix \mathbf{X}^{\star} is recovered statistically from MLE, we compare $\Phi(\mathbf{X})$ and $\Phi(\bar{\mathbf{X}})$ by resorting to a widely used statistical distance, known as the Hellinger distance, which was defined in (2). The vector entrywise formula of the Hellinger distance is given as

$$d_{H}^{2}\left(\Phi\left(\boldsymbol{X}\right),\Phi(\bar{\boldsymbol{X}})\right) = \frac{1}{m}\sum_{j=1}^{m}d_{H}^{2}\left(\Phi\left(\mu_{j}-\lambda_{j}\right),\Phi(\bar{\mu}_{j}-\lambda_{j})\right),$$
(59)

where $\{\bar{\mu}_j\}$ is the estimated version of $\{\mu_j\}$ obtained from (57). As was previously observed, by increasing the value of SNR, Noisy OPeRA performs better in terms of the NMSE . A similar behavior occurs with the Hellinger distance shown in Fig. 12. The Hellinger distance is obtained is very small for all SNR values in this experiment, However, it is decreasing for an increasing SNR, which appears to confirm the recovery of the desired matrix in statistical (noisy) environments by taking advantage of a large number of samples—thus without considering the rank-one and the PSD constraints.

To show the sustained benefit of sample abundance in the noisy case, we compare Noisy OPeRA with *Noisy PhaseLift*

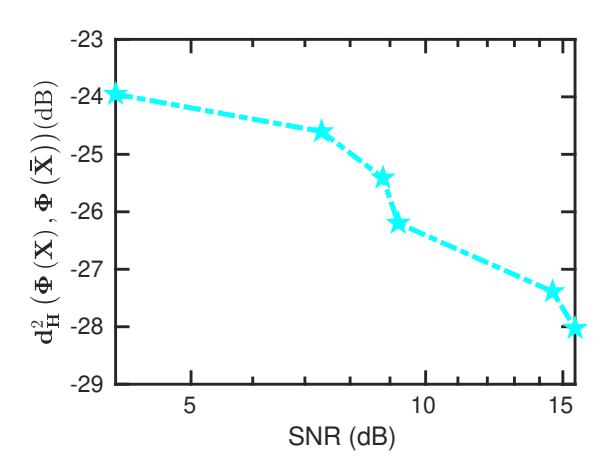


Figure 12: Comparing the CDF of the desired matrix $\Phi(X)$ and the CDF of the recovered matrix $\Phi(\bar{X})$ using the Hellinger distance (59). Although the Hellinger distance of our estimation is very small overall, it shows a decreasing behavior as the SNR grows large.

Table IV: Comparing Noisy PhaseLift and Noisy OPeRA in terms of CPU time and NMSE.

Noisy PhaseLift [23]	m = 5000	m = 10000	m = 20000
CPU time (s)	1.4698	2.0305	3.7529
NMSE	0.0045	0.0041	0.0035
Noisy OPeRA	m = 5000	m = 10000	m = 20000
CPU time (s)	0.9497	1.4436	2.3137
NMSE	0.0040	0.0015	3.8875e-04

formulation firstly introduced in [23] as

$$\min_{\boldsymbol{\mu}, \boldsymbol{X}} - \Upsilon_{\boldsymbol{\mu}}(\boldsymbol{X}) + \alpha \operatorname{Tr}(\boldsymbol{X})$$
s.t. $\mu_{j} = \operatorname{Tr}(\boldsymbol{V}_{j}\boldsymbol{X}), \quad j \in \mathcal{J},$

$$\boldsymbol{X} \succeq 0,$$
(60)

where $\Upsilon_{\mu}(X) = \log(f(s|\mu))$, with the noisy measurement vector $\{s_i\}$ is sampled from a probability distribution $f(.|\mu)$, and α is a positive scalar. For our numerical examinations, we assume the measurement noise is distributed as $\mathbf{z} \sim \mathcal{N}\left(0,0.25 \boldsymbol{I}_{m}\right)$ and the termination criterion is $\left\|\boldsymbol{X}_{i}-\boldsymbol{X}^{\star}\right\|_{\mathrm{F}}^{2} \leq 5 \times 10^{-3} \left\|\boldsymbol{X}^{\star}\right\|_{\mathrm{F}}^{2}$. Table IV shows that by using a large number of samples (and making rank-one and PSD constraints redundant) in the noisy one-bit sampling scenario, Noisy OPeRA can recover the signal with a better CPU time for sample sizes $m \in \{5000, 10000, 20000\}$ compared to the noisy PhaseLift method. This is similar to our discussion in the noiseless scenario; see Section V. Interestingly, by growing the number of samples, the NMSE is enhanced more significantly by Noisy OPeRA than that of the noisy PhaseLift method. The results are averaged over 5 experiments. The settings of the input signal, time-varying thresholds and the sensing are also chosen in the same way as in Section III-C.

VIII. CONCLUSION

We showed that the abundance of samples that naturally occurs in one-bit sampling scenarios has significant implications in lowering the computational cost of phase retrieval by making costly constraint redundant. The problem then boils down to a set of linear inequalities that may be solved by RKA within the proposed OPeRA signal recovery framework. The numerical results showcased the effectiveness of the proposed approaches for phase retrieval.

REFERENCES

- [1] R. P. Millane, "Phase retrieval in crystallography and optics," *J. Opt. Soc. Am. A*, vol. 7, no. 3, pp. 394–411, Mar 1990.
- [2] W. Kim and M. H. Hayes, "The phase retrieval problem in x-ray crystallography," in *Proceedings of the Acoustics, Speech, and Signal Processing*, 1991. ICASSP-91., 1991 International Conference, USA, 1991, ICASSP '91, p. 1765–1768, IEEE Computer Society.
- [3] J. R. Fienup, J. C. Marron, T. J. Schulz, and J. H. Seldin, "Hubble space telescope characterized by using phase-retrieval algorithms," *Appl. Opt.*, vol. 32, no. 10, pp. 1747–1767, Apr 1993.
- [4] J. E. Krist and C. J. Burrows, "Phase-retrieval analysis of pre- and post-repair hubble space telescope images," *Appl. Opt.*, vol. 34, no. 22, pp. 4951–4964, Aug 1995.
- [5] A. M. Sarnik, "Phase retrieval: A practical application for the space telescope," in *Inverse Optics II*, R.H.T. Bates and A. J. Devaney, Eds. International Society for Optics and Photonics, 1985, vol. 0558, pp. 85 – 94, SPIE.
- [6] R. W. Gerchberg and W. O. Saxton, "Phase determination for image and diffraction plane pictures in the electron microscope," *Optik*, vol. 34, pp. 275–284, 1971.
- [7] R. W. Gerchberg and W. O. Saxton, "A practical algorithm for the determination of phase from image and diffraction plane pictures," *Optik*, vol. 35, pp. 227–246, 1972.
- [8] J. R. Fienup, "Comments on "the reconstruction of a multidimensional sequence from the phase or magnitude of its Fourier transform"," *IEEE Transactions on Acoustics, Speech, and Signal Processing*, vol. 31, no. 3, pp. 738–739, Jun 1983.
- [9] J. R. Fienup, "Phase retrieval algorithms: a comparison," Appl. Opt., vol. 21, no. 15, pp. 2758–2769, Aug 1982.
- [10] J. R. Fienup, "Reconstruction of an object from the modulus of its Fourier transform," *Opt. Lett.*, vol. 3, no. 1, pp. 27–29, Jul 1978.
- [11] E. J. Candes, T. Strohmer, and V. Voroninski, "PhaseLift: Exact and stable signal recovery from magnitude measurements via convex programming," *Communications on Pure and Applied Mathematics*, vol. 66, no. 8, pp. 1241–1274, 2013.
- [12] E.J. Candès and X. Li, "Solving quadratic equations via PhaseLift when there are about as many equations as unknowns," *Foundations of Computational Mathematics*, vol. 14, no. 5, pp. 1017–1026, 2014.
- [13] K. Jaganathan, S. Oymak, and B. Hassibi, "Sparse phase retrieval: Convex algorithms and limitations," in 2013 IEEE International Symposium on Information Theory. IEEE, 2013, pp. 1022–1026.
- [14] E. J. Candès, X. Li, and M. Soltanolkotabi, "Phase retrieval via Wirtinger flow: Theory and algorithms," *IEEE Transactions on Information Theory*, vol. 61, no. 4, pp. 1985–2007, Apr 2015.
- [15] Y. Chen and E. J. Candes, "Solving random quadratic systems of equations is nearly as easy as solving linear systems," in *Advances* in *Neural Information Processing Systems* 28, pp. 739–747. Curran Associates, Inc., 2015.
- [16] R. Kolte and A. Özgür, "Phase retrieval via incremental truncated wirtinger flow," ArXiv, vol. abs/1606.03196, 2016.
- [17] H. Zhang, Y. Liang, and Y. Chi, "A nonconvex approach for phase retrieval: Reshaped Wirtinger flow and incremental algorithms," *Journal* of Machine Learning Research, vol. 18, no. 141, pp. 1–35, 2017.
- [18] S. Nayer and N. Vaswani, "Sample-efficient low rank phase retrieval," IEEE Transactions on Information Theory, vol. 67, no. 12, pp. 8190–8206, 2021.
- [19] F. Fogel, I. Waldspurger, and A. d'Aspremont, "Phase retrieval for imaging problems," *Mathematical programming computation*, vol. 8, no. 3, pp. 311–335, 2016.
- [20] G. Jagatap and C. Hegde, "Fast, sample-efficient algorithms for structured phase retrieval," Advances in Neural Information Processing Systems, vol. 30, 2017.
- [21] S. Bahmani and J. Romberg, "Phase retrieval meets statistical learning theory: A flexible convex relaxation," in *Artificial Intelligence and Statistics*. PMLR, 2017, pp. 252–260.
- [22] H. Sahinoglou and S. D. Cabrera, "On phase retrieval of finite-length sequences using the initial time sample," *IEEE Transactions on Circuits* and Systems, vol. 38, no. 8, pp. 954–958, 1991.

- [23] E. J. Candes, Y. C. Eldar, T. Strohmer, and V. Voroninski, "Phase retrieval via matrix completion," *SIAM review*, vol. 57, no. 2, pp. 225– 251, 2015.
- [24] A. Eamaz, F. Yeganegi, and M. Soltanalian, "Modified arcsine law for one-bit sampled stationary signals with time-varying thresholds," in ICASSP 2021-2021 IEEE International Conference on Acoustics, Speech and Signal Processing (ICASSP). IEEE, 2021, pp. 5459–5463.
- [25] Texas Instruments, "Analog embedded processing," Active Filter Design Techniques, Literature Number SLOA088 Texas Instruments, excerpted from OP-Amps for Everyone, Literature Number SLOD006A.
- [26] A. Mezghani and A. L. Swindlehurst, "Blind estimation of sparse broadband massive MIMO channels with ideal and one-bit ADCs," *IEEE Transactions on Signal Processing*, vol. 66, no. 11, pp. 2972–2983, 2018.
- [27] S. Sedighi, B. Shankar, M. Soltanalian, and B. Ottersten, "One-bit DoA estimation via sparse linear arrays," in *IEEE International Conference on Acoustics, Speech and Signal Processing (ICASSP)*. IEEE, 2020, pp. 9135–9139.
- [28] A. Eamaz, F. Yeganegi, and M. Soltanalian, "Covariance recovery for one-bit sampled data with time-varying sampling thresholds—Part I: Stationary signals," TechRxiv, 2022.
- [29] A. Eamaz, F. Yeganegi, and M. Soltanalian, "Covariance recovery for one-bit sampled data with time-varying sampling thresholds—Part II: Non-stationary signals," TechRxiv, 2022.
- [30] C. Qian and J. Li, "ADMM for harmonic retrieval from one-bit sampling with time-varying thresholds," in 2017 IEEE International Conference on Acoustics, Speech and Signal Processing (ICASSP). IEEE, 2017, pp. 3699–3703.
- [31] C. Gianelli, Luzhou Xu, Jian Li, and Petre Stoica, "One-bit compressive sampling with time-varying thresholds for sparse parameter estimation," in 2016 IEEE Sensor Array and Multichannel Signal Processing Workshop (SAM). IEEE, 2016, pp. 1–5.
- [32] P. Wang, J. Li, M. Pajovic, P. T. Boufounos, and Philip V Orlik, "On angular-domain channel estimation for one-bit massive MIMO systems with fixed and time-varying thresholds," in 51st Asilomar Conference on Signals, Systems, and Computers. IEEE, 2017, pp. 1056–1060.
- [33] F. Xi, Y. Xiang, S. Chen, and A. Nehorai, "Gridless parameter estimation for one-bit MIMO radar with time-varying thresholds," *IEEE Transactions on Signal Processing*, vol. 68, pp. 1048–1063, 2020.
- [34] J. M. Ortega, Numerical analysis: a second course, SIAM, 1990.
- [35] M. A. Davenport, Y. Plan, E. Van Den Berg, and M. Wootters, "1-bit matrix completion," *Information and Inference: A Journal of the IMA*, vol. 3, no. 3, pp. 189–223, 2014.
- [36] L. Vandenberghe and S. Boyd, "Semidefinite programming," SIAM review, vol. 38, no. 1, pp. 49–95, 1996.
- [37] Y. Nesterov, Introductory lectures on convex optimization: A basic course, vol. 87, Springer Science & Business Media, 2003.
- [38] C. F. Van Loan and G. Golub, "Matrix computations (Johns Hopkins studies in mathematical sciences)," 1996.
- [39] J. Briskman and D. Needell, "Block Kaczmarz method with inequalities," *Journal of Mathematical Imaging and Vision*, vol. 52, no. 3, pp. 385–396, 2015.
- [40] D. Leventhal and A. S. Lewis, "Randomized methods for linear constraints: convergence rates and conditioning," *Mathematics of Oper*ations Research, vol. 35, no. 3, pp. 641–654, 2010.
- [41] T. Strohmer and R. Vershynin, "A randomized Kaczmarz algorithm with exponential convergence," *Journal of Fourier Analysis and Applications*, vol. 15, no. 2, pp. 262–278, 2009.
- [42] L. Dai, M. Soltanalian, and K. Pelckmans, "On the randomized Kaczmarz algorithm," *IEEE Signal Processing Letters*, vol. 21, no. 3, pp. 330–333, 2013.
- [43] H. Chernoff, "A measure of asymptotic efficiency for tests of a hypothesis based on the sum of observations," *The Annals of Mathematical Statistics*, pp. 493–507, 1952.
- [44] H. Chernoff, "A career in statistics," Past, Present, and Future of Statistical Science, vol. 29, 2014.
- [45] S. A. Bhaskar and A. Javanmard, "1-bit matrix completion under exact low-rank constraint," in 2015 49th Annual Conference on Information Sciences and Systems (CISS). IEEE, 2015, pp. 1–6.



Arian Eamaz (Student Member, IEEE) received the B.Sc. degree in electrical and computer engineering from the Amirkabir University of Technology, Tehran, Iran, in 2019. He is currently working toward the Ph.D. degree in electrical and computer engineering with the University of Illinois Chicago, Chicago, IL, USA. His research interests include applied mathematics, statistical signal processing, statistics and optimization theory. He is a Member of American Statistical Association-ASA and IEEE Information Theory Society. He was the recipient of

2019 best B.Sc. thesis award and prestigious 2021 Wexler Award.



Farhang Yeganegi received the B.Sc. degree in electrical and computer engineering from the Amirkabir University of Technology, Tehran, Iran, in 2019. He is currently working toward the Ph.D. degree in electrical and computer engineering with the University of Illinois Chicago, Chicago, IL, USA. His research interest include optimization theory, statistics, numerical linear algebra and statistical signal processing. He was the recipient of 2019 best B.Sc. thesis award.



Mojtaba Soltanalian (Senior Member, IEEE) received the Ph.D. degree in electrical engineering (with specialization in signal processing) from the Department of Information Technology, Uppsala University, Sweden, in 2014. He is currently with the faculty of the Electrical and Computer Engineering Department, University of Illinois at Chicago (UIC), Chicago, IL, USA. Before joining UIC, he held research positions with the Interdisciplinary Centre for Security, Reliability and Trust (SnT, University of Luxembourg), and California Institute of Tech-

nology, Pasadena, CA, USA. His research interests include interplay of signal processing, learning and optimization theory, and specifically different ways the optimization theory can facilitate a better processing and design of signals for collecting information, communication, and also to form a more profound understanding of data, whether it is in everyday applications or in large-scale, complex scenarios. Dr. Soltanalian serves as an Associate Editor for IEEE Transactions on Signal Processing and as the Chair of the IEEE Signal Processing Society Chapter in Chicago. He was the recipient of the 2017 IEEE Signal Processing Society Young Author Best Paper Award, an also the 2018 European Signal Processing Association Best PhD Award.